Effect of Cavitation Water Jet Peening on 8090Al-li Fatigue Life N/cycle

JOSEPH SEKYI-ANSAH*[1], JAMES KWASI QUAISIE[3], STEPHEN EDUKU[5], PHILIP BAIDOO[2], , PHILIP YAMBA[3] FELIX UBA[4], ENOCK A. DOUDU[2] EMMANUEL AMANKWAH[4].

[1]Dept. of Mechanical Engineering, Takoradi Technical University, Takoradi, 00233, GHANA
[2] Faculty of Technology, University of Education Winneba, Kumasi 00233, GHANA
[3] Faculty of Engineering, (Welding & Fabrication Dept.) Tamale Technical University, Tamale 00233, GHANA
[4] School of Engineering, University of Energy & Natural Resource, Sunyani 00233, GHANA
[5]Dept. of Electrical & Electronics Engineering, Takoradi Technical University, Takoradi, 00233, GHANA

Abstract: Numerous pressure process parameters were used to cavitation strengthen Aluminum lithium alloy (8090Al-Li). We used cavitation water jet peening to extend the fatigue life N/cycle of an 8090 lithium aluminium alloy (8090Al-li) over an unpeened sample. Surface morphology, compressive residual stress (CRS), and microhardness increase to 4,699μm, -147MPa, and 173HV with a 30 MPa peened area CWJP pressure increment. This is demonstrated by the data. The CWJP induces CRS in the 8090Al-li, which increases its resistance to fatigue crack growth (FCG), fatigue crack initiation (FCI), and fatigue striation, while also decreasing the dimple size. When the strain was influenced, the fatigue life of 8090al-li was increased by 61.9965 %, 91.89 %, and 111.74 %, respectively. The study details the fatigue N/cycle of 8090Al-Li using CWJP.

Keywords: CWJP; fatigue N/cycle; fatigue striation; residual stress; aluminium-lithium 8090 alloy

Received: May 15, 2022. Revised: October 19, 2022. Accepted: November 13, 2022. Published: December 28, 2022.

1. Introduction

Cavitation occurs when the local pressure in the liquid surpasses the saturated vapour pressure, resulting in cavitation of the phase transformation. Cavitation was discovered to be a detrimental occurrence in the early days because hydraulic equipment such as propellers, turbines, and pumps caused significant damage, resulting in varying degrees of efficiency loss based on cavitation power. However, as more research on cavitation behaviour has been conducted, it has been discovered that cavitation is indeed suitable in a variety of applications. Due to the cavitation bubble's clouding development and the high pressures varying on the solid surface wall caused by the cavitation jet, the jet's presence grows primarily due to high stress and nozzle diameter. A cavitation bubble's descent in particular [1] can be formed, causing fragile materials to shatter swiftly. Additionally, cavitation bubbles that collapse may generate high-velocity shock waves. Cavitation shot peening increases the fatigue strength of metals like laser shot peening. Due to the absence of injection, this process is referred to as “cavitation shotless" [2] or simply " shotless peening " [3]. This results in a compressive residual tension being applied to the material. Surface roughness is reduced significantly during cavitation peening compared to traditional peening [4]. Another advantage of cavitation peening is that it can be used to treat patients in remote places. Sheet flexure fatigue experiments, on the other hand, were utilized to validate the fatigue strength of duralumin plates by cavitation peening holes. Aeronautical items such as application components with attachment holes should be subjected to tensile fatigue testing to ensure that they are not only stress-bending but also stress-stretching. In the event of cavitation peening, cavitation bubbles can be formed by introducing a high-speed water jet into the water-filled

cavity. [6]. Aluminium alloys have been extensively reinforced because of their high plasticity, high strength, and light weight, and a large number of aluminium alloys are employed due to their properties, but fatigue fracture is one of the primary causes, due to the high strength of air. Numerous surface treatments have already been performed, (e.g., laser shock peening (LSP), shot peening (SP), and others. [7-12], which extends the life of aerospace materials used in harsh cryogenic environments and increases fatigue life. Additionally, this approach has limitations in terms of application in the aerospace industry (pollution, high cost, etc.).

A resource-efficient manufacturing process CWJP is a novel methodology that promotes enhanced fatigue life (N/C), improved technologies, and corrosion-resistant materials. 13–14. Cavitation damage is induced by shock waves and microjets when a high number of bubbles continuously collapse [15, 16], which often occurs on the component's surface [17, 18]. These techniques can help increase the performance of the surface. Numerous research groups have identified numerous mechanical surface modification approaches for increasing the fatigue strength of aluminium alloys [19]. Among these, the most extensively used method for improving the fatigue strength of aluminium alloys for aerospace purposes was shot peening (SP). Due to the presence of their CRS, Hammond discovered that the SP treatment enhanced the fatigue life of an aluminium alloy 7075 surface during rotating bending [20]. Benedetti et al. [5] also investigated the beneficial effects of shot-peening treatments on the inverse fatigue bending of smooth and notched aluminium 7075 alloy specimens and found that the enhancement in fatigue properties following SP treatment was particularly pronounced for notched specimens [21]. Additionally, they evaluated the residual stress distribution near shot-peened notches using finite element analysis and a novel method based on micro X-ray diffraction measurements, and their recommendation indicated that CRS could be enhanced by increasing the sharpness of the notched. [8]. Oguri [22] compared the fatigue life enhancement of aluminium 7075 alloys using shot peening fine particles (SPFP) and standard SP, utilizing ceramic particles with a diameter of 50m. His findings revealed that the fatigue life of FPSP samplings was orders of magnitude larger than that of samplings treated with standard SP. [9] According to Inoue et al. [23], fatigue life increased on the aluminium alloy 7075 following SPFP, mostly due to the crack site's initiation of migration from the surface to the sub-surface due to the surface's high CRS. Rujian et al. [11] also evaluated the tensile control, microstructure, and RS properties of additive created wire arc aluminium alloy 2319 using laser peening (LP) and discovered that the addition of CRS and grain refinement caused by LP enhanced micro hardness and tensile qualities. According to S. Huang et al. [24], identified the influence of LP on the various energies on fatigue fracture of aluminium 6061-T6 alloy and observed that tensile fatigue was significantly improved. Additionally, cryogenic treatment (CT) can drastically alter the microstructure of treated materials, resulting in increased hardness, wear resistance, and material strength. 25; 26. Zhou et al. [27] LP also evaluated the qualities of aluminium alloy 2024-T351, including CT fatigue properties, fatigue testing, and fatigue morphologies. Their experiment reveals that both LP and CT may be utilized to improve the qualities of the aluminium fatigue alloy 2024T351, while Sekyi-Ansah et al. study the surface properties and damage produced by water jet peening processing in the alloy 8090Al-Li. It was discovered that the surface roughness, residual stress, and erosion all had a substantial effect on the 8090al-li alloy. The surface depth decreased in proportion to the increase in pressure and the severity of the impact [28]. Quaisie and co. also conducted a study on the use of different incident pressures

during micro forming water jet shock and confirmed that the hardness measurements revealed a slight increase in hardness along the cross-section of the moulded area during the cold-rolled condition of the sample and a significant increase in hardness along the cross-section of the annealed 304 stainless steel foils [29]. Various effects on the fatigue life N/cycle and microstructures of metal components have been investigated using a variety of LSP and CWJP settings and materials. However, no CWJP data on 8090 Al-Li parts have been published, which is why this work will examine the fatigue life N/cycle efficiency of the CWJP alloy as well as the fatigue-striation morphological mechanisms using electron microscopy (SEM) and strength. On this basis, the FCG enhancement process is discussed. Additionally, the findings were dependent upon the N/cycle increase in the hardness of peened and unpeened metal samples.

2. Methodology

2.1 Preparation of Materials

Throughout the test, thick plates of 8090 aluminium-lithium alloy (8090Al-Li) were used. Table 1 and Table 2 detail the mechanical properties and chemical composition of 8090Al-Li. The first set of four samples was cut into a dog-bone form and the dimensions are indicated in Figure 1, while the second sample was cut into four 50 x 50 mm (length x width) square bars with a 4 mm thickness. All samples were collected using electro-discharge equipment capable of severing wires. Each sample was selected and polished using 600#, 800#, 1000#, 2000#, and 2500# sandpapers, followed by a polishing treatment using the ASIDA-YM22 sandpaper polishing machine, followed by cleaning and drying with water and alcohol. The fatigue test piece with parameters was confirmed in Figure 1.

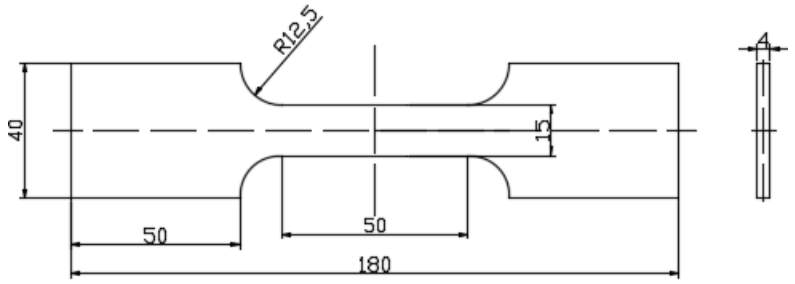

Figure 1. Fatigue test sample and parameters (unit: mm)

Table 1 Mechanical Properties of Aluminum-Lithium 8090 alloy

Mechanical Property	Yield Stress Strength (MPa)	Tensile Strength (MPa)	Poisson's Ratio (υ)	Elongation (%)	Elastic Modulus (GPa)
value	90	300	0.33	13	67

Table 2 Chemical composition of Aluminum-Lithium 8090 alloy

Element	Al-li	Cu	Mg	Fe	Zn	Si	Zr	Mn	Cr	Ti	Residuals
Mass Fraction	2.2~2.7	1.0~1.6	0.6~1.3	0	0.25	0	0.040~0.16	0.1	0	0	0

2.2 Experimental design

The test team used cavitation shot peening machines to experiment. The machine operated at a flow rate of about 14 L/min at a pressure of 50 MPa overall. The peening period for cavitation was 20 min and the distance (S) from the dump to the surface of the sample was 100 mm. On the top of the tank, the level of free liquids was set at 60 cm, guaranteeing that the free liquid level did not interfere with the water jet peening. The cavitation extension of the experimental device for water jet expansion (Figures 1a and b). For 24 hours, tap water was held at a temperature of 20 ± 2 °C in a large tank. The experiment was conducted in a transparent tank. The nozzle utilized in this test was intended for angular nozzles, which have a 1.5 mm throat diameter, a 12 mm throat length, and a 20° extended angle, as illustrated in Figure 2.

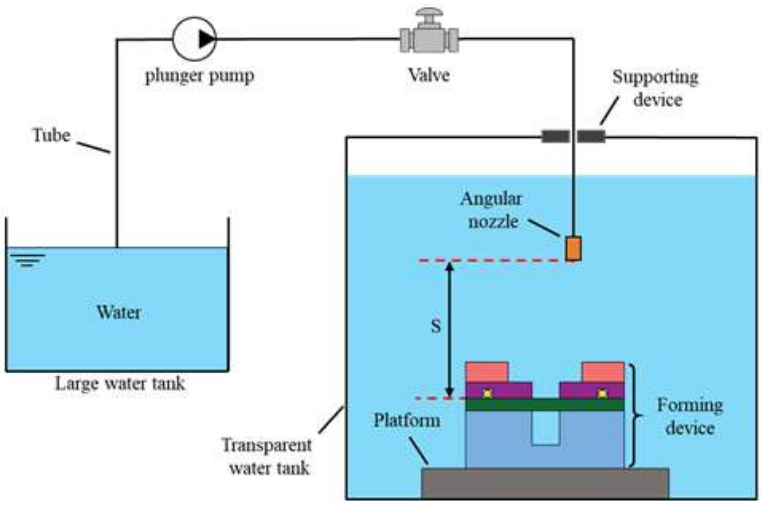

Figure 1(a): Water-jet cavitation experimental system

Figure 1(b): Block diagram of water-jet cavitation experimental system

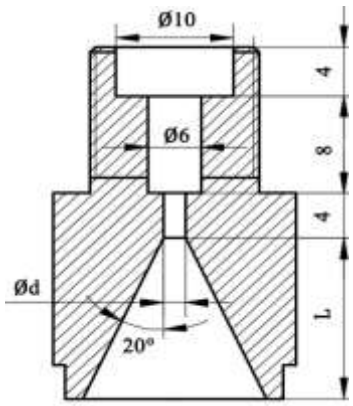

Figure 2: Nozzle geometry diagram.

2.3 Measurements of residual stress

The layer of the sample residual stress measurement on the CRS of the sample before and after CWJP was done using an X-ray diffraction (XRD) machine with a $\sin^2\Psi$ method and a beam diameter of 1 mm, where ψ was varied from 0.0^0, 25.0^0, 35.0^0, and 45.0^0. The current, voltage and counting times were 6.0 mA, 22.0 kV, and 0.50 sec, respectively. The diffraction phase is the α phase (311) plane and the X-ray source is the Cu-K α ray. The feed angle for ladder scanning was 0.10^0/s. The stress constant K was -166MPa/ (^{0}). The scanning start and end angles were set at 136^0 and 1430. Electrolytic polishing was employed for the removal of the specimen layer by layer to acquire the required depth profile for the CRS test of 8090Al-Li.

2.4 Micro hardness

The hardness provides resistance to mechanical indentation, abrasion, and scraping with the least amount of plastic deformation attainable. When handling cavitation peening water, the micro-hardness analyzer machine HXD-1000TMSC/LCD was used to determine the surface hardness. The ASTM E92-82 standard was used to conduct the test. There was a 1.96N and a 10s load. For the microhardness analyzer, the surface sample diamond indentation, and the

Vickers hardness test theory to be determined and demonstrated, the estimates were obtained from their midpoints. Microhards are classified into four types and three primary measurements based on the DIN EN ISO 6507-1 and BS 5411-6 indications. To begin with, a perfectly regulated test force is used to drive the diamond pyramid indenter into the sample. The test force was maintained for approximately 10~20s. Following the stay period, the diamond pyramid indenter is evacuated, leaving a faint trace of an indent on the metallic surface of the sample, which appears square moulded.

2.5 Roughness of the surface

This experiment utilizes the laser microscope 3D and profile measurement (KEYENCE, VK-K250) model made in Japan. Profile roughness measurement on CWJP samples at peened and unpeened

regions along lateral and transverse (L, T) directions was measured with a surface profilometer to investigate surface features.

2.6 Fatigue fracture test evaluation

To investigate the mechanism of fatigue life N/cycle boost, the fatigue fracture morphology of 8090Al-Li with CWJP and varied peening pressures was studied. The fatigue fracture of 8090Al-Li dog-bone pieces was cut by EDM and prepared by ASIDA-YM22 before being cleaned with an ultrasonic cleaning machine to prevent oil pollution, the influence of CWJP on FCG propagation, and the fatigue life N/cycle performance of 8090Al-Li. At room temperature, and MTS-809 servo-hydraulic system with a frequency of 10 Hz and a sine wave was used. The stress ratio ($R=\sigma min /\sigma max$ was kept constant at 0.1. A maximum tensile force of 300kN was applied to the 8090Al-Li with and without CWJP. The fatigue fracture was distinguished by (SEM).

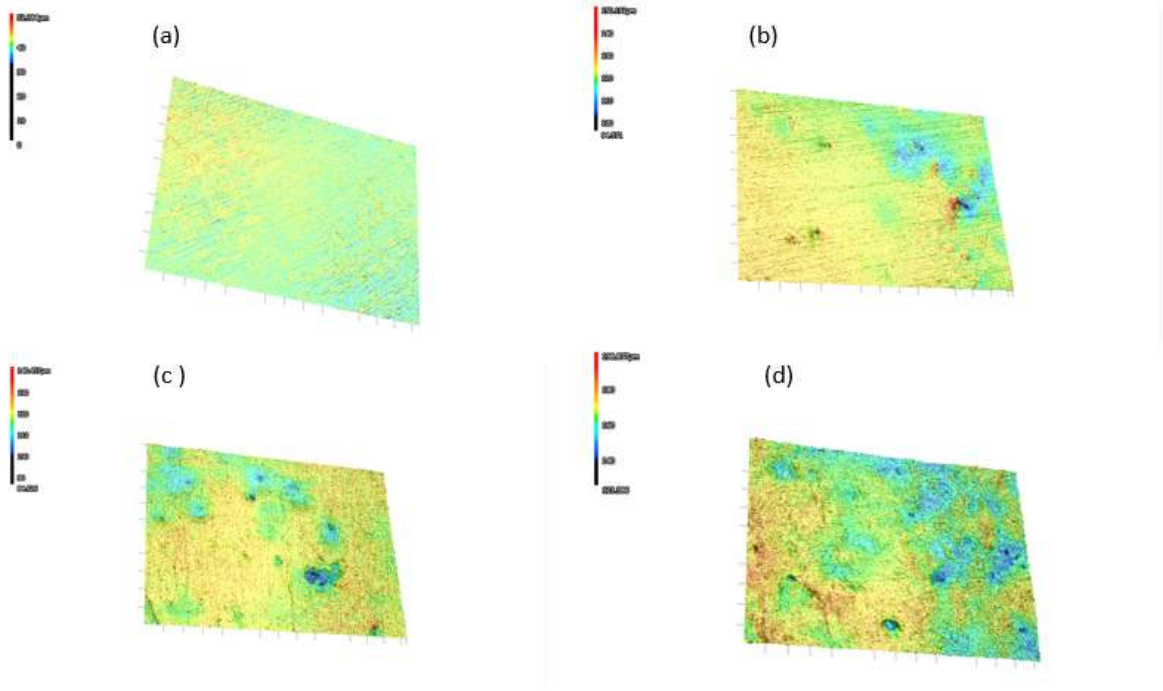

Figure.4i. 3D surface contour roughness; (a) Unpeened, (b) 20MPa, (c) 25MPa, and (d) 30MPa.

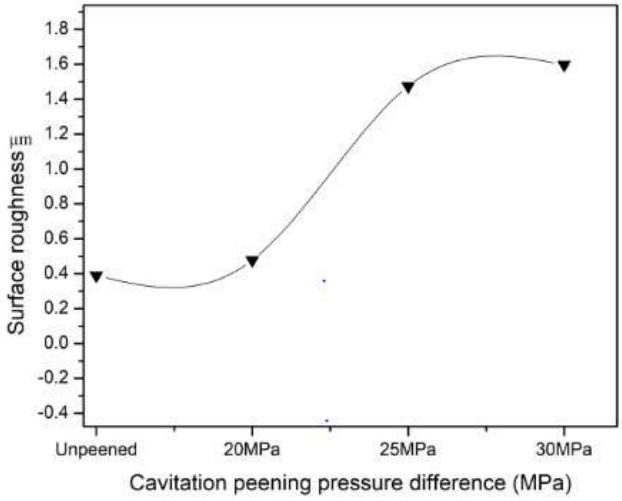

Figure 4ii Curve of surface roughness

3. Result And Discussion

3.1 Surface Morphology

Figures 4i(a)-d) exhibit the 3D microscope and the profile measurement (KEYENCE VK-K250) that represent the 3D-surface contour of the samples and the cross-sectional roughness 8090Al-Li, and Figure 4ii displays its curve. The surface of the microscope is for all samples. The value of the unpeened raw surface sample Ra of 0.390μm, as seen in figures 4a, b, c, and D, with roughness values of 0.478μm, 1.475μm, and 1.597μm, was presented in the pit sample density size of figure 4ii, while the percentage of roughness was improved by 22.56 %, 278.21 %, and 309.48 %, respectively, with impact pressures of 20, 25, and 30 MPa. Surface roughness is a useful evaluation metric for mechanical coordination, corrosion resistance, and manufacturing resistance. The depth of the CWJP CRS surface increases fatigue life N/cycle and fracture closure, lowering the stress strength factor, forming consistent micro pits, improving metal roughness, and causing stress levels. Fatigue cracks related to surface roughness have an impact on the major aspects of aerodynamic performance. It is one of the primary indicators used to evaluate the component's production [31, 32]. When we use CWJP to stabilize the surface, the roughness disappears as well. The first feature of CWJP is its effect on operational peen pressure. The ideal pressure emphasizes the peening effect. The topography and surface hardness of CWJP have a significant impact. Secondly, by establishing geometric parameters and an operating strain structure, the CWJP method specifies the effect of cavitation occurrences on the metal surface structure.

3.2 Surface Hardness

As seen in Figure 5. The initial hardness of samples of 8090 lithium alloy is 120 HV. According to Figure 5, the hardness increases from 20MPa, 25MPa, and 30MPa to 158,6HV, 168.2HV, and 173HV with a proportion of 32,167 %, 40.17 %, and 44.17 %, respectively, in comparison to unpeend. Figure 5 depicts how micro-hardness improves with increasing peening pressure. The rate of micro hardness expansion, at either extreme, increases with pressure [33]. The more dislocated entanglements result in the hardening of work on the closed surface, the density of the dislocation walls is dislodged, the dislocation in enclosures reaches a peening value, and the dislocation materials, are reorganized into fresh walls, enhancing the grain to refine the material of a top surface. Thus, CWJP efficiently improves surface microhardness by 8090Al-Li; however, the increase in microhardness and amplitude is verified as the impact pressure increases. CWJP objectives outperform traditional objectives in terms of CP and SOPWP [34, 35].

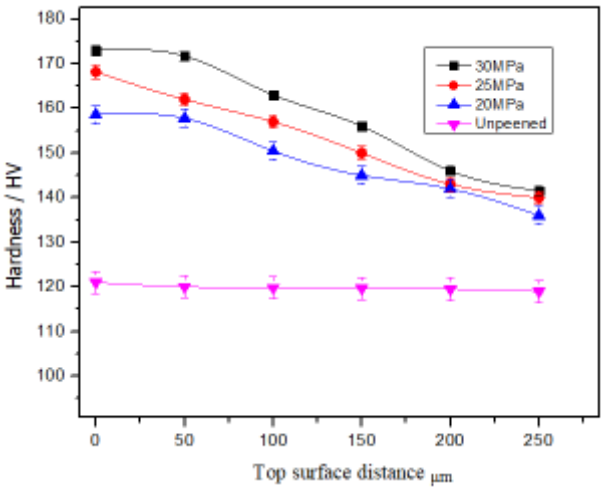

Figure 5 Vickers hardness curves of 8090 aluminum-lithium alloy with different peening pressure

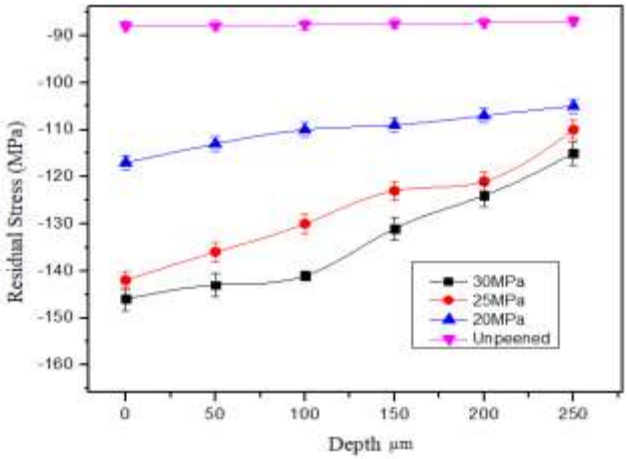

Figure 6 Distribution of residual stress field of 8090 aluminium alloy lithium with different pressure

3.3 Distribution of residual stress

Figure 6 depicts the compressive residual stress (CRS) of an 8090Al-Li sample with varying peening pressure, constant distance, and cavitation duration WJP when S= 100 mm and T= 10 min. Soyama et al. examined CRS in the wall enclosing the whole [5] residual stresses to inhibit fatigue crack development and fatigue life. Fu and co. certifies its metal material strength, which determines the effects on residual stress and hardness level. [36, 37] [38] formalized paraphrase Figure 6 shows that the CRS of CWJP sample 8090Al-Li is increased by -117MPa, -142MPa, and -147MPa, with CRS of 34.090%, 61,363%, and 67.045% compared to the non-peened sample, -88MPa, as the CRS induced by CWJP in the close-surface layer leads to pressure progressions at the 8090 Al-Li bearing region. As a result, the presence of CRS of CWJP in the close-superface layer increases. When the fatigue amplitude of the material decreases, the CRS in the closed surface layer increases fatigue striation and fatigue N/cycle, lowering the FCG propagation tangible stress strength factor. CWJP enhances the surface and depth of the 8090Al-Li CRS with N-cycle fatigue, substantially reducing the negative effect of fatigue stretching tensile stress.

3.4 Fatigue life N/cycle

The fatigue of the unpeened sample is N/cycle 10999, and the fatigue life cycle is extended to 17818, 21106, or 23389 by 61.9965% by 91.89%, and 111.74% by 111.74%, respectively, as pressure is adjusted to 20 MPa, 25 MPa, and 30 MPa. CWJP is induced by residual stresses and hardness, which are significant for fatigue enhancements N/cycle of metal structures because they lower the stress strength intensity factor (K). Table 3 has also been improved in terms of fatigue life N/cycle action. Furthermore, with CWJP P=30MPa, 80,90Al-Li had the highest fatigue life N/cycle because of the higher compression residual stress and grain refining circulation caused by the CWJP. I. Bantounas et al [39] discussed the impact of CRS on tiredness in life. The results also revealed that fatigue cracks were mostly induced by a sector of highest machining stress, but fatigue development might also be delayed by compressive cavitation peening stress (CP), C. Masuda and colleagues [22] demonstrated that a high number of in-depth penetration residual stresses per CP develops fatigue strength.

Figures 7(a) and 7 (b) show the fatigue crack cycle for a sample under the CWJP effect (b). Here, we observe the incubation time for plastic deformation without mass loss in the area of fatigue. There was no peening when the incubation period was over. [5]. After the incubation period, cavitation erosion begins. CWJP had higher residual stresses and erosive wells than unpeened tests.

Table 3 Fatigue life Cycle results for Peened and Unpeened

CWJP	Mean Fatigue Life Sample	Percentage of Fatigue N/Cycle compared to unpeened
Unpeened	10999	-
20MPa	17818	61.9965
25MPa	21106	91.89
30MPa	23389	111.74

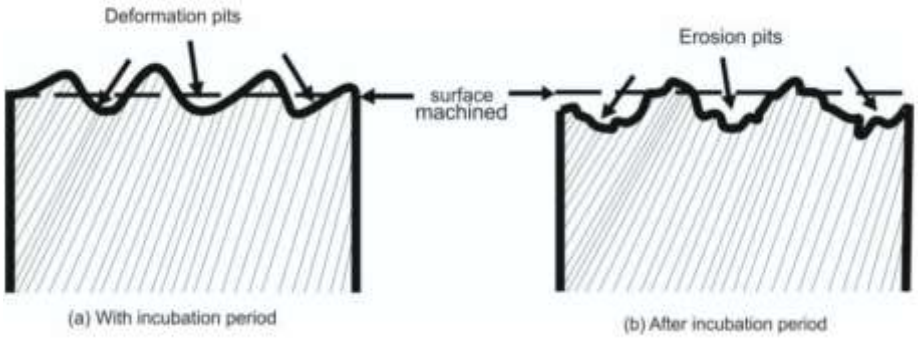

Figure 7. Schematic diagram of the surface within and after the incubation period.

3.5 Fatigue Fracture Morphology

Figure 8a depicts how load and pressure are concentrated in the simplest and most vulnerable region, leading to the initiation of a fatigue crack (FCI). According to Figures 8 b, c, and d, peened samples took longer than unpeened samples to propagate FCG; fatigue cracks originated from fractured samples, and micro-cracks grew gradually before being promptly ruptured at the crack of the unpeened samples. It delays the immediate pressures on the sample induced by the compressive residual stress (CRS) caused by the fatigue crack propagation (FCP) zone before the fracture occurs. In addition to fracture propagation, tensile stress causes crack nucleation along the border of the crack. In addition, when RS is introduced, the CWJP sample grows steadily around the core. Figure 8b shows that if the P = 20 MPa crack-growing region becomes stable, the crack-initiating corner of a peened sample spreads somewhat into the sample body. The first peened sample crack began in the upper-left corner and progressed to the middle before eventually failing. Case in Point (8c) The steeper angle in the figure is where fatigue fracture occurs when the CRS layer is present after a CWJP and final failure (8d). To maximize stress concentrations, peening at P = 30 MPa results in an area with peak stresses of 30 MPa where stresses are concentrated in a crisp, rectangular, angular region. In their study [40], Hatamleh et al. investigated surface layer stress and fatigue limitations. An increase in the cavitation peening pressure leads to an increase in metallic compressive residual stress, which in turn leads to a rise in fatigue N /cycle sample time.

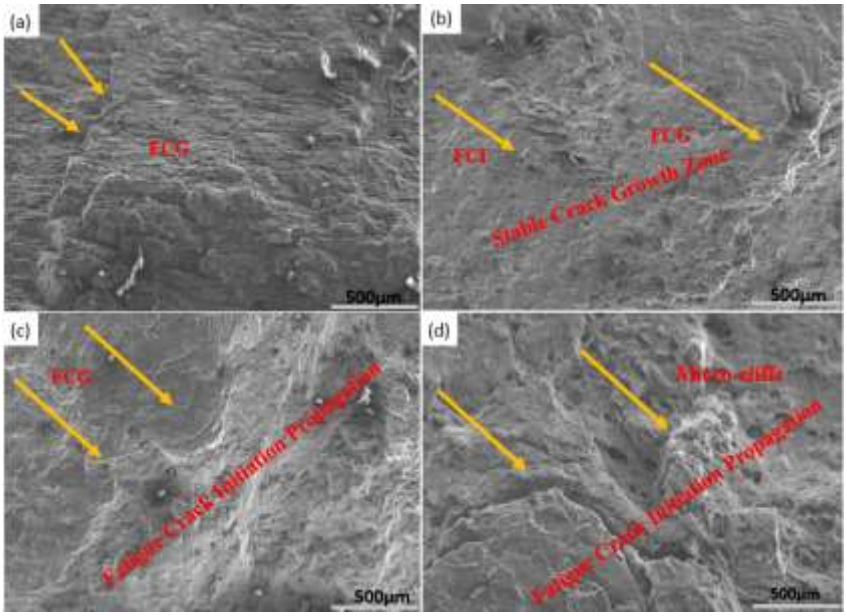

Figure. 8. Fatigue fracture Morphology of cavitation water jet peening at different pressures (a) unpeened, (b) 20 MPa, (c) 25MPa, and (d) 30MPa.

3.7 Fatigue crack behaviors and fracture surface microstructure CWJP

Unpeened sample cracks have an extension intrados of fatigue boards that are parallel to one another but perpendicular to the fracture channel, as seen in figure (9a). A linear surface of secondary crack material has also been added, as shown in figure 9. (9b). This peels in the sample's perpendicular direction, capturing partial tensile stress and delaying the spread of FCG in a peened sample that seeks to show larger fatigue density, high inclusion, and an increase in micro-cliff when compared to an unpened sample at P = 20 MPa. Upon recurrent and cyclic stress cracking, the form and striation transition indicates the direction of material damage. For the crack to become stable, the peening pressure causes the break to enlarge over time, and the mid-thickness of the fracture surface region of the specimen reveals interior cracks. As the fracture length rises, the distance between fatigue striations widens. As a result, the fatigue cracks rise to the fracture point as a result of this process. The FCG rate in the stretchy with more micro-cliffs observed along the fatigue crack path and extremely wide scales of laid-back FCG rate in the peened sample with more micro-cliffs that were observed along the fatigue crack path and somewhat larger dimples in the figure is higher in the peened sample. A P = 25 MPa peening sample shows an internal fracture zone's stress level. In terms of metallurgical effects on grain orientation and SIF alterations, striation space is altered [42]. The narrow parallel grooves curved in the surface segment of the metal fractures displaying striations, fatigue fracture ridges, and sample inclusions have been confirmed by SEM findings. An expel of (9d) results in fewer dimples with less inclusion of tear ridges, and this results in an angular fracture zone that develops quickly under high pressure. The stress of external loading exceeds the yield power of the material,

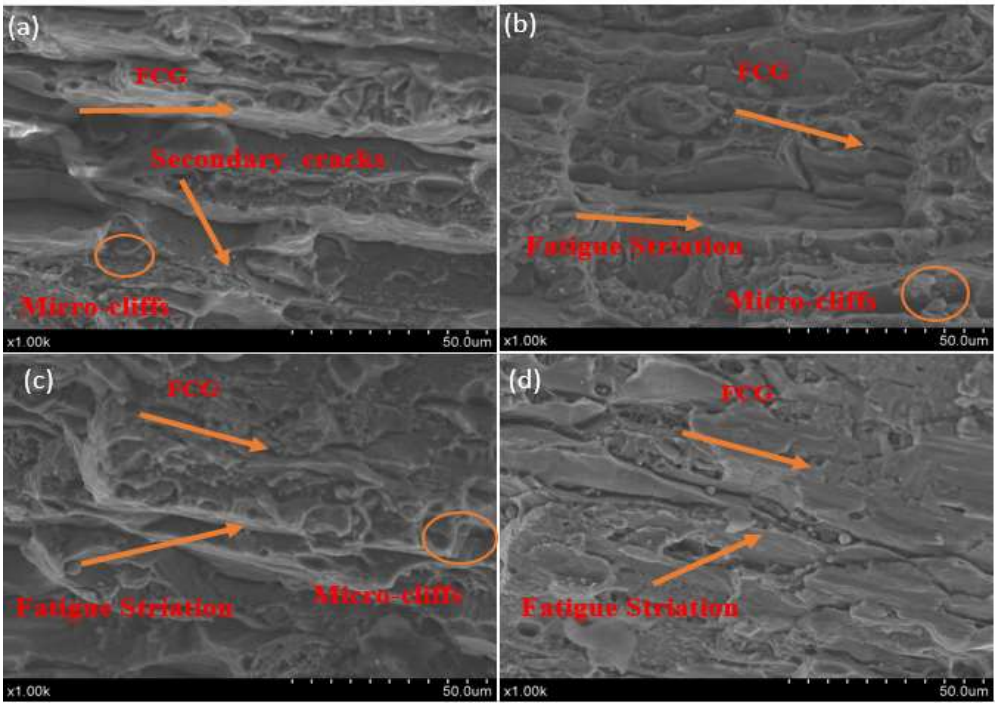

Figure. 9 Fatigue striation of different pressures of cavitation water jet peening. (a) Unpeened (b) 20MPa, (c) 25MPa and (d) 30MPa.

resulting in plastic deformation that alters the fatigue crack patterns. This phase is characterized by an increase in striation and micro-cavities morphing into isometric dimples on fracture surfaces, as well as an increase in compressive and stress levels along the micro-cavity [43].

3.8 Final fracture morphology

Both unpeened and peened samples are shown in figure 10, although the dimples in 10a are much larger than those in 10b, 10c, and 10d, which are all peened samples. Before fracturing, the cavitation causes compressive stress, which deforms the grain structure and improves its mechanical properties. Dimple growth is seen in figures (10b & c), which is corroborated in figure (10d) by the presence of slide steps and lateral cracks on the dimple's lateral surface under the impact of 25MPa to 30 MPa, which suggests that severe plastic deformation occurred before fracture. Because of this, the harshness of cyclical loads increases. Fracture fatigue striation and the FCI position are linked to the CWJP's metallic characteristics. The FCI position and fatigue striation of the fatigue fracture is affected by fatigue fracture striations in the material crack direction. These studies reveal that CWJP reduces fatigue from the metallic and subsurface of N/cycle, FCG, and FCI positions. 8090Al-fatigue Li's striation is altered by the higher peening friction.

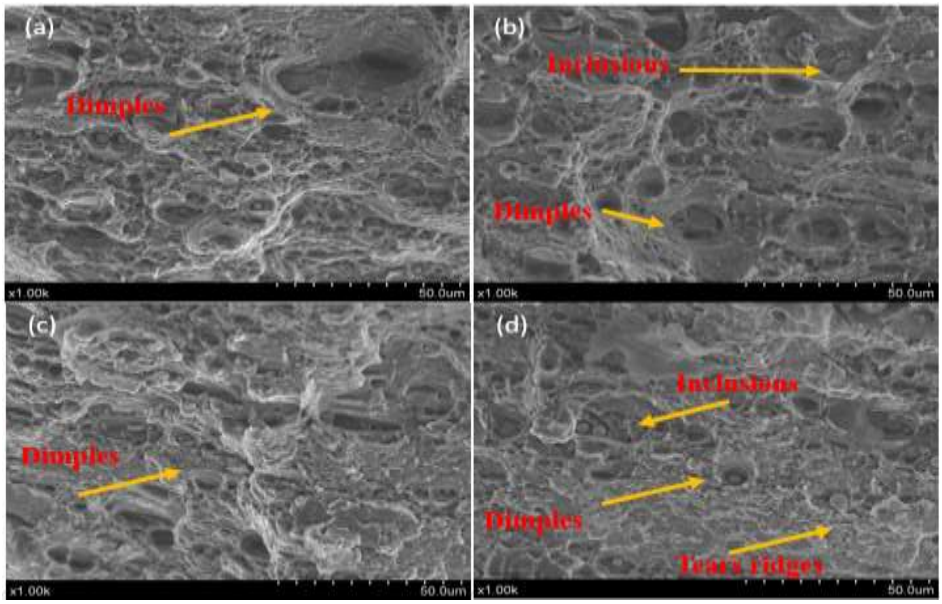

Figure 10 Fracture Morphology of Dimples Coalescence Different Pressures of Cavitation Water Jet Peening. (a) Unpeened (b) 20MPa, (c) 25MPa and (d) 30MPa.

4. Conclusions

This study examined the effect of CWJP peening pressure on the fatigue N/cycle of 8090Al-Li. CWJP's effect on 8090Al-micro hardness, roughness, fatigue fracture properties, fatigue crack striation, and residual stress was discussed. As a result, the following findings were made:

- ✓ Greater peening pressure has increased the fatigue life N/cycle of 8090 Al-Li, which illustrates CWJP's capacity to extend the life of the material.
- ✓ Surface morphology improved by 22.56%, 278.21%, and 309.48% in 8090Al-Li from 20 to 25 and 30 MPa, respectively. Unpeened samples had higher residual stress due to increased CWJP-induced fatigue N/cycle in CRS and lower stress levels.
- ✓ Due to CWJP-induced work hardening and grain enhancement, the micro hardness of the 8090Al-Li with CWJP-30MPa increased by 44.16% compared to the unpeened sample.
- ✓ Several factors contribute to an increase in the operative stress strength of 8090Al-fatigue striation. Between 20, 25 and 30MPa, the fatigue life N/cycle was raised by a total of 61.9965%, 91.899%, and 111.74%, respectively.
- ✓ A fracture relocation occurs in the FCI and FCG regions, causing fatigue striation patterns to change. Pressure changes for peening efficiently prevent the formation of fatigue cracks and increase fatigue N/Cycle.

Acknowledgements

Our thanks to the experts who have contributed to the development of the research work. The effort that we have put into this report would not have been possible without the support and help of many individuals. We would like to extend our sincere thanks to all of them.

References

[1] A. A. Aganin, M. A. Il'gamov, L. A. Kosolapova, and V. G. Malakhov, "Collapse of a spheroidal cavitation bubble near a solid

wall," *Russian Aeronautics (Iz VUZ),* vol. 59, pp. 190-196, 2016/04/01 2016.

[2] H. Soyama, K. Saito, and M. Saka, "Improvement of fatigue strength of aluminum alloy by cavitation shotless peening," *Journal of engineering materials and technology,* vol. 124, pp. 135-139, 2002.

[3] H. Soyama, *Enhancing the aggressive intensity of a cavitating jet by introducing a cavitator and a guide pipe* vol. 9, 2013.

[4] H. Soyama, "Introduction of compressive residual stress using a cavitating jet in air," *J. Eng. Mater. Technol.,* vol. 126, pp. 123-128, 2004.

[5] H. Soyama and F. Takeo, "Comparison between cavitation peening and shot peening for extending the fatigue life of a duralumin plate with a hole," *Journal of Materials Processing Technology,* vol. 227, pp. 80-87, 2016/01/01/ 2016.

[6] H. Soyama, Y. Yamauchi, Y. Adachi, K. Sato, T. Shindo, and R. Oba, *High-Speed Observations of the Cavitation Cloud around a High-Speed Submerged Water Jet* vol. 38, 1995.

[7] S. P. Gadag, M. N. Srinivasan, and B. L. Mordike, "Effect of laser processing parameters on the structure of ductile iron," *Materials Science and Engineering: A,* vol. 196, pp. 145-154, 1995/06/15/ 1995.

[8] O. Hatamleh, J. Lyons, and R. Forman, "Laser and shot peening effects on fatigue crack growth in friction stir welded 7075-T7351 aluminum alloy joints," *International Journal of Fatigue,* vol. 29, pp. 421-434, 2007/03/01/ 2007.

[9] K. Li, Y. Hu, and Z. Yao, "Experimental study of micro dimple fabrication based on laser shock processing," *Optics & Laser Technology,* vol. 48, pp. 216-225, 2013/06/01/ 2013.

[10] D. Ju, H. Tsuda, V. Ji, T. Uchiyama, and R. Oba, *Residual stress improved by water jet peening for a quenched gear* vol. 25, 2004.

[11] W. Yun, B. Philip, X. Zhenying, and W. Junfeng, "Study on fatigue crack growth performance of EH36 weldments by laser shock processing," *Surfaces and Interfaces,* vol. 15, pp. 199-204, 2019/06/01/ 2019.

[12] G. Sun, R. Zhou, J. Lu, and J. Mazumder, "Evaluation of defect density, microstructure, residual stress, elastic modulus, hardness and strength of laser-deposited AISI 4340 steel," *Acta Materialia,* vol. 84, pp. 172-189, 2015/02/01/ 2015.

[13] G. Chen, L. Lu, C. Ren, and X. Ge, "Temperature dependent negative to positive strain rate sensitivity and compression behavior for 2024-T351 aluminum alloy," *Journal of Alloys and Compounds,* vol. 765, pp. 569-585, 2018.

[14] M. Prudhomme, F. Billy, J. Alexis, G. Benoit, F. Hamon, C. Larignon, *et al.*, "Effect of actual and accelerated ageing on microstructure evolution and mechanical properties of a 2024-T351 aluminium alloy," *International Journal of Fatigue,* vol. 107, pp. 60-71, 2018.

[15] I. Akhatov, O. Lindau, A. Topolnikov, R. Mettin, N. Vakhitova, and W. Lauterborn, "Collapse and rebound of a laser-induced cavitation bubble," *Physics of Fluids,* vol. 13, pp. 2805-2819, 2001.

[16] M. Ijiri, D. Shimonishi, D. Nakagawa, and T. Yoshimura, "New water jet cavitation technology to increase number and size of cavitation bubbles and its effect on pure Al surface," *International Journal of Lightweight Materials and Manufacture,* vol. 1, pp. 12-20, 2018/03/01/ 2018.

[17] E. Hutli, T. Fekete, and M. Nedeljkovic, "Surface characteristics and cavitation damage progress in ductile materials," *Engineering Failure Analysis,* vol. 106, p. 104157, 2019/12/01/ 2019.

[18] R. E. A. Arndt, "Vortex Cavitation," in *Fluid Vortices*, S. I. Green, Ed., ed Dordrecht: Springer Netherlands, 1995, pp. 731-782.

[19] D. Hammond and S. Meguid, "Crack propagation in the presence of shot-peening residual stresses," *Engineering Fracture Mechanics,* vol. 37, pp. 373-387, 1990.

[20] J. Li, A. Feng, J. Zhou, H. Chen, Y. Sun, X. Tian, *et al.*, "Enhancement of fatigue properties of 2024-T351 aluminum alloy processed by cryogenic laser peening," *Vacuum,* vol. 164, pp. 41-45, 2019/06/01/ 2019.

8090Al–Li Alloy by Using Cavitation Water Jet Peening Processing," *Iranian Journal of Science and Technology, Transactions of Mechanical Engineering,* vol. 45, pp. 299-309, 2021.

[21] M. Benedetti, V. Fontanari, B. Winiarski, M. Allahkarami, and J. Hanan, "Residual stresses reconstruction in shot peened specimens containing sharp and blunt notches by experimental measurements and finite element analysis," *International Journal of Fatigue,* vol. 87, pp. 102-111, 2016.

[22] K. Oguri, "Fatigue life enhancement of aluminum alloy for aircraft by Fine Particle Shot Peening (FPSP)," *Journal of Materials Processing Technology,* vol. 211, pp. 1395-1399, 2011.

[23] A. Inoue, T. Sekigawa, K. Oguri, T. Tagawa, and T. Ishikawa, "Mechanism of fatigue life improvement due to fine particle shot peening in high strength aluminum alloy," *Journal of the Japan Institute of Metals,* vol. 74, pp. 370-377, 2010.

[24] J. Sheng, S. Huang, J. Zhou, J. Lu, S. Xu, and H. Zhang, "Effect of laser peening with different energies on fatigue fracture evolution of 6061-T6 aluminum alloy," *Optics & Laser Technology,* vol. 77, pp. 169-176, 2016.

[25] K. Gu, B. Zhao, Z. Weng, K. Wang, H. Cai, and J. Wang, "Microstructure evolution in metastable β titanium alloy subjected to deep cryogenic treatment," *Materials Science and Engineering: A,* vol. 723, pp. 157-164, 2018.

[26] G. Wang, K. Gu, Z. Huang, and P. Ding, "Improving the wear resistance of as-sprayed WC coating by deep cryogenic treatment," *Materials Letters,* vol. 185, pp. 363-365, 2016.

[27] J. Zhou, J. Li, S. Xu, S. Huang, X. Meng, J. Sheng*, et al.*, "Improvement in fatigue properties of 2024-T351 aluminum alloy subjected to cryogenic treatment and laser peening," *Surface and Coatings Technology,* vol. 345, pp. 31-39, 2018/07/15/ 2018.

[28] J. Sekyi-Ansah, Y. Wang, J. K. Quaisie, F. Li, C. Yu, E. Asamoah*, et al.*, "Surface Characteristics and Cavitation Damage in

[29] J. K. Quaisie, W. Yun, X. Zhenying, Y. Chao, F. Li, P. Baidoo*, et al.*, "Experimental Study on Water-Jet Shock Microforming Process Using Different Incident Pressures," *Advances in Materials Science and Engineering,* vol. 2020, 2020.

[30] J. M. Papazian, G. G. Bott, and P. Shaw, "Effects of lithium loss on strength and formability of aluminum-lithium alloys 8090 and 8091," *Materials Science and Engineering,* vol. 94, pp. 219-224, 1987/10/01/ 1987.

[31] A. Azhari, C. Schindler, and B. Li, "Effect of waterjet peening on aluminum alloy 5005," *The International Journal of Advanced Manufacturing Technology,* vol. 67, pp. 785-795, 2013/07/01 2013.

[32] F. Echouchene, H. Belmabrouk, L. Le Penven, and M. Buffat, "Numerical simulation of wall roughness effects in cavitating flow," *International Journal of Heat and Fluid Flow,* vol. 32, pp. 1068-1075, 2011/10/01/ 2011.

[33] W. Oliver and G. M. Pharr, *Measurement of hardness and elastic modulus by instrumented indentation* vol. 19, 2004.

[34] C. Masuda, S. Nishijima, and Y. Tanaka, *Relationship between fatigue strength and hardness for high strength steel* vol. 52, 1986.

[35] S. G. Pantelakis, P. V. Petroyiannis, K. D. Bouzakis, and I. Mirisidis, "Surface hardness increase of 2024 aluminum alloy subjected to cyclic loading," *Theoretical and Applied Fracture Mechanics,* vol. 48, pp. 68-81, 2007/08/01/ 2007.

[36] C. Montross, T. Wei, L. Ye, G. Clark, and Y. W. Mai, *Laser Shock Processing and its Effects on Microstructure and Properties of Metal Alloys: A Review* vol. 24, 2002.

[37] J. M. Yang, Y. C. Her, N. Han, and A. Clauer, *Laser shock peening on fatigue behavior of 2024-T3 Al alloy with fastener holes and stopholes* vol. 298, 2001.

[38] J. Fu, Y. Zhu, C. Zheng, R. Liu, and Z. Ji, *Effect of laser shock peening on mechanical*

properties of Zr-based bulk metallic glass vol. 313, 2014.

[39] I. Bantounas, D. Dye, and T. C Lindley, *The role of microtexture on the faceted fracture morphology in Ti–6Al–4V subjected to high-cycle fatigue* vol. 58, 2010.

[40] C. Gu, J. Lian, Y. Bao, and S. Münstermann, "A microstructure sensitive modeling approach for fatigue life prediction considering the residual stress effect from heat treatment," *Procedia Structural Integrity,* vol. 13, pp. 2048-2052, 2018/01/01/ 2018.

[41] S. P. Kuo, S. S. Kuo, and O. S. P. R. B. C. Northrop Grumman Space Technology, "Theoretical study of plasma effect on a conical shock wave," 2006-03-15 2006.

[42] O. Hatamleh, J. Lyons, and R. Forman, *Laser and shot peening effects on fatigue crack growth in friction stir welded 7075-T7351 aluminum alloy joints* vol. 29, 2007.

[43] X.-q. Zhang, L.-s. Chen, X.-l. Yu, L.-s. Zuo, and Y. Zhou, "Effect of laser shock processing on fatigue life of fastener hole," *Transactions of Nonferrous Metals Society of China,* vol. 24, pp. 969-974, 2014/04/01/ 2014.

[44] S. G. Pantelakis, P. V. Petroyiannis, K. D. Bouzakis, and I. Mirisidis, *Surface Hardness Increase of 2024 Aluminum Alloy Subjected to Cyclic Loading* vol. 48, 2007.